Building Simulation

Seventh International IBPSA Conference
Rio de Janeiro, Brazil
August 13-15, 2001

VALIDATION AND APPLICATION OF THE DAYLIGHT SOURCE MODEL BASED ON GEOSTATIONAL METEOROLOGICAL SATELLITE IMAGES

Yoshiaki Uetani
(uetani@fuarc.fukuyama-u.ac.jp)
Fukuyama University, Faculty of Engineering, Department of Architecture
Fukuyama 729-0292, JAPAN

ABSTRACT

This paper examines the precision of a statistical model to estimate global and beam irradiance and illuminance at hourly intervals by the three channels of the geostational meteorological satellites images. The multiple liner regression analysis is performed between the satellites image values and instantaneous illuminance and irradiance measured at the Fukuyama University. By the weather condition analysis, causes reducing the precision are studied. The daylight source model is applied to estimate the geographical distribution of daylight availability.

INTRODUCTION

Both daylighting simulation tools and daylight availability data for various weather conditions are essential to design an architecture with energy efficiency and luminous environment of good quality. Though there are useful daylighting simulation tools being developed in the world, daylight source models are insufficient for the needs for both research and practice.

Existing databases and numerical models on solar radiation and daylight availability are usually based on the measured data by surface observations at the limited number of meteorological observatories and daylighting measurement stations. Because of the financial difficulty to set up and operate such a station, the solar radiation and daylight availability data incline to the cities and countries where national meteorological observatories or major research institutes are located. To solve the dispersion problem, a new meteorological database for building design has recently been developed in Japan [1]. The database provides estimated solar radiation and other meteorological data measured at 842 Automated Meteorological Data Acquisition System (AMeDAS) throughout the country at intervals of approximately 21 kilometers.

Satellite-derived solar energy models

As the alternative approaches of surface observations, researchers have developed statistical models [2] and physical models [3] to estimate the solar energy resources using the visual channel of meteorological satellite images. The statistical approaches have been developed to be a major project [4, 5]. It was applied to simulations of solar energy system [6] and the daylighting data web server [7, 8]. An improved statistical method estimates global, diffuse, beam solar radiation and illumination [9].

There are three advantages of the satellite-derived solar energy information over the surface observed products. The first is the quasi-realtime availability of the current solar energy data. The geostational meteorological satellite scans the globe and transfers the images to the ground every hour. An end user with the appropriate receiving system is able to receive and utilize the hourly satellite images. Secondly, an satellite image covers all over the hemisphere of the globe. A disk image covers not only Japan but eastern Asia, western Pacific and Oceania, though the fringe of the disk, e.g. the Arctic region, is useless due to the distortion. Once a satellite-derived solar energy model is developed in Japan, it is expected to be applied to other countries covered by the satellite. Third, a pixel on a satellite image corresponds to the area of about 7 kilometers square in Japan. The resolution is much smaller than existing databases or models based on the surface observation, on the other hand it should be noted that the satellite-derived value is the average of the square.

Another statistical model for global and beam solar radiation and illumination

The author proposed another statistical model for global and beam solar radiation using the images of Japanese geostational meteorological satellite GMS-5 [10, 11]. The model is based on the multiple linear regression analysis to estimate surface observed hourly cumulative global and beam radiation values from the satellite observed image values. The major difference of the model and the traditional statistical methods above mentioned is that it utilizes the three channels of meteorological satellite images. The visual channel, the only one used in the traditional method, is converted to the albedo representing the optical thickness of cloud. The infrared channel corresponds to the height of cloud deck. The water vapor channel approximates the relative humidity of the troposphere. The combination of three channels have been expected to provide more detailed information on the atmosphere than ever.

The satellite derived global and beam horizontal irradiance values are converted into the diffuse and beam horizontal illuminance by the luminous efficiency of sky light and sun light on the assumption that the instantaneous data is equal to the average in the period.

The precision of estimated irradiance was expressed as

a root mean square difference (RMSD) and a mean bias difference (MBD). The percent RMSD and MBD values for the global irradiance were 24% and 0.1%, while those for the beam horizontal irradiance were 55% and 0.9%. The difference of the time period of measurements was considered as one of the reasons of relatively low precision of the beam horizontal irradiance. The surface observed values are hourly cumulative radiation, while a pixel value on the satellite image is measured instantaneously by the satellite that rotates in 100 revolutions per minute. A method to improve the correlation with the cumulative irradiance is to utilize the average of surrounding pixels instead of one pixel which corresponding the location [4]. Unfortunately, this is less useful for the daylighting simulation, because instantaneous global and beam illuminance values are required to estimate the worst scenario of luminous environment, as well as the cumulative values to estimate energy savings. The better solution would be the utilization of surface observed instantaneous global and beam radiation and illumination data synchronized with the satellite scanning.

This paper examines the precision of the proposed statistical model to estimate global and beam irradiance and illuminance using geostational meteorological satellite images. The multiple liner regression analysis is performed between the satellites image values and instantaneous illuminance and irradiance measured at the Fukuyama University. By the weather condition analysis, causes reducing the precision are studied. As an application of the model, geographical distribution of global illuminance and beam horizontal illuminance are estimated.

IMAGES OF THE GEOSTATIONAL METEOROLOGICAL SATELLITE: GMS-5

There are five geostational meteorological satellites above the equator observing the globe: METEOSAT (0˚E), GOMS (76˚E), GMS (140˚E), GOES (135˚W) and GOES (75 ˚W). In this paper, the images observed by the Japanese geostational meteorological satellite GMS-5 are utilized. GMS-5 is stationary at the altitude of 35800 kilometers above the equator, 140 degrees of east longitude. GMS-5 rotates in 100 revolutions per minute and scans the globe from the North Pole to the South Pole in 25 minutes every hour.

An array of four visual sensors (VIS channel: 0.50~0.75 μm) captures an image of 13376 x 10000 pixels with 6 bit depth. Each of three infrared sensors (IR1 channel: 10.5~11.5 μm, IR2 channel: 11.5~12.5 μm, IR3 channel: 6.5~7.5 μm) captures an image of 6688 x 2500 pixels with 8 bit depth. The theoretical resolutions on the surface right under the GMS-5 are 1.25km/pixel for the visual sensor array and 5km/pixel for each of the infrared sensors. The captured signals are transferred in realtime to the data acquisition center located in a suburb of Tokyo and provided for weather forecasts and other applications.

In the following regression analysis, the off-line data of GMS images [12] are utilized. The coordinate transformation of the globe images produces square images surrounded by two pairs of latitudes (20˚N and 50˚N) and longitudes (120˚E and 150˚E). VIS, IR1, and IR3

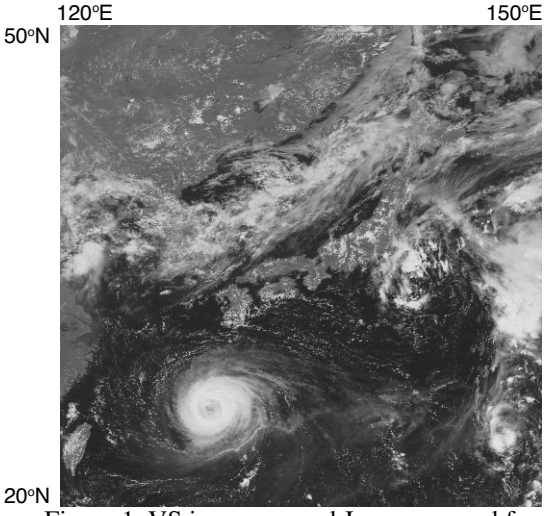

Figure 1 VS image around Japan scanned from 11:34:48AM to 11:39:42AM on Aug 7, 2000

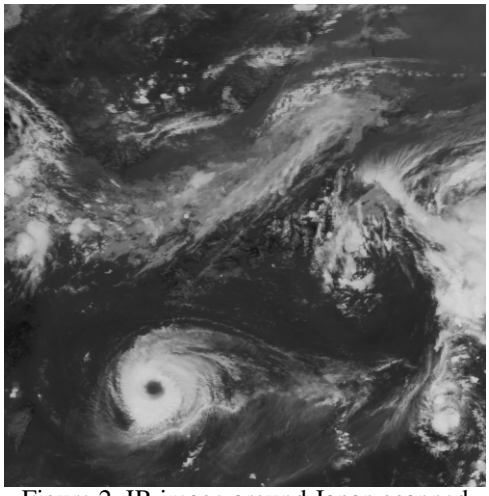
Figure 2 IR image around Japan scanned simultaneously with Figure 1

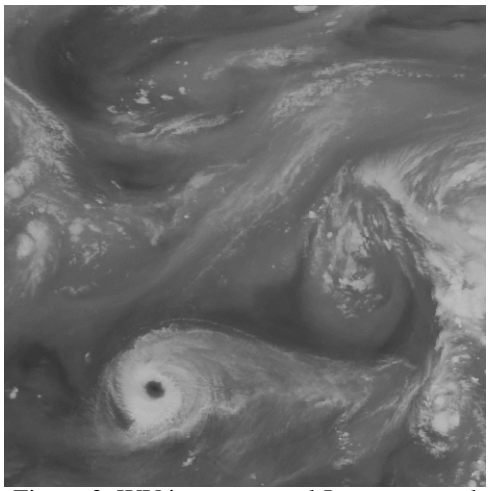
Figure 3 WV image around Japan scanned simultaneously with Figure 1

channels are referred as VS (**Figure 1**), IR (**Figure 2**), and WV (**Figure 3**) images respectively.

Visible image (VS) provides us a view of the earth close to the human sense with the highest spatial resolution [13]. Each pixel of the visible image is converted into the albedo by the calibration data provided with the image. Infrared image (IR) is the most familiar image on weather forecast programs. Each pixel is converted into the equivalent black body temperature by the provided calibration data. The temperature by the infrared image corresponds to the height of cloud deck as the atmosphere cools with height. Infrared images are usually inverted so that the colder cloud appears brighter and the warmer land and sea appear darker in presentation. Water vapor image (WV) represents the radiation in water vapor absorption bands. The image shows the highest clouds but swirls cover lands and seas. Each pixel is converted into the equivalent black body temperature distributions by the provided calibration data as IR channel.

VALIDATION OF THE MODEL

Preliminary Analysis for All Weather Condition

The previous study analysed the hourly cumulative global irradiance and beam normal irradiance observed at the Fukuoka Meteorological Observatory (130˚23'E, 33˚35'N) from July 1, 1996 to June 30, 1997 [10, 11]. The analysis in this paper utilizes the instantaneous data to examine the difference of the time period of measurements in the model. The global and beam normal irradiance and illuminance data were observed synchronizing with the satellite scanning from November 25, 1999 to October 31, 2000 at the Fukuyama University (133˚15'E, 34˚30'N) using the instruments of the meteorological monitoring station shown in **Figure 4**. A normal incidence pyrheliometer and a normal incidence illuminance meter mounted on an automated solar tracker measure the beam normal irradiance I_{oBN} [W/m^2] and beam normal illuminance E_{oBN} [klx]. The aperture half angle of both the beam normal sensors is 2.5 degrees. A pyranometer on the solar tracker and an illuminance meter behind measure global irradiance I_{oG} [W/m^2] and global illuminance E_{oG} [klx]. A data logger collects data every minute from above solar sensors, as well as a silicon photovoltaic pyranometer, a quantum sensor, thermometer, ventilated air temperature/humidity meters, and an ultrasonic anemoscope/anemometer. The surface observed instantaneous beam horizontal irradiance I_{oBH} [W/m^2] and illuminance E_{oBH} [klx] were derived by multiplying the beam normal components and the sine of solar elevation angle $\sin h_s$.

Figure 4 The automated solar tracker, pyranometer and global illuminance meter

For the satellite observed images, the off-line data with calibration data [12] are utilized as mentioned above. The theoretical resolution of the satellite images at the location of the Fukuyama University is 6.7 km/pixel. The calibration tables attached to each image convert the raw pixel values of the VS image (Figure 1), IR image (Figure 2), and WV image (Figure 3) into albedo A_{VS} [-], equivalent black body temperature T_{bIR} [K] and T_{bWV} [K] respectively. The albedo A_{VS} depends on the solar elevation angle h_s because it is defined as the ratio of the beam normal solar irradiance at the satellite to the irradiance reflected on the surface and received by the satellite. In the model, the albedo A_{VS} is normalized to the normalized albedo $A_{nVS.}$

$$A_{nVS} = A_{VS} / \sin h_s \qquad (1)$$

The surface observed instantaneous data and satellite observed data are combined together to be a database. The quality control procedure by the following criteria reduces the data sets to 2954 cases,

(a) the solar elevation angle h_s beyond 5˚,

(b) A_{nVS}, T_{bIR}, T_{bWV}, I_{oG}, I_{oBN}, I_{oBH} and are all valid.

The multiple linear regression equations are examined to estimate instantaneous global irradiance I_{eG} [W/m^2] and beam horizontal irradiance I_{eBH} [W/m^2].

$$I_{eG} = k_G + b_{1,G} A_{nVS} + b_{2,G} T_{bIR} + b_{3,G} T_{bWV} + b_{4,G} \sin h_s \qquad (2)$$

$$I_{eBH} = k_B + b_{1,B} A_{nVS} + b_{2,B} T_{bIR} + b_{3,B} T_{bWV} + b_{4,B} \sin h_s \qquad (3)$$

Table 1 shows the multiple regression coefficients as the result of preliminary analysis for all weather condition on both cumulative irradiance [MJ/m^2 h] and instantaneous irradiance [W/m^2]. In the analysis of the beam horizontal irradiance, the extreme cases of low beam normal irradiance (I_{oBN} < 6 W/m^2) are rejected. The number of valid cases on each weather condition is shown in Table 1. The comparison of the measured and estimated instantaneous global irradiance I_{oG} and I_{eG} by the preliminary analysis are plotted in **Figure 5**. The measured and estimated beam horizontal irradiance I_{oBH} and I_{eBH} are shown in **Figure 6**.

Table 2 shows the precision of the multiple regression models. The precision expressed by the percent RMSD values for hourly cumulative irradiance are 26% on the global and 60% on the beam component. The precision for instantaneous irradiance are 41% for the global and 54% for the beam component. The overall precision agrees with the elaborate model based on visual

Table 1 Coefficients of the multiple regression models of irradiance

			Cases	R^2	k	B_1	B_2	B_3	B_4
Cumulative irradiance [MJ/m²h] from July 1,'96 to June 30,'97 at Fukuoka Meteorological Observatory	Global	All weather	2576	0.802	-2.46E+0	-1.91E+0	4.67E-3	5.70E-3	3.07E+0
		Clear	741	0.866	8.89E-2	-2.70E+0	NS	NS	3.65E+0
		Fine	806	0.842	-2.32E+0	-2.99E+0	NS	1.05E-2	3.44E+0
		Cloudy	1019	0.661	-2.73E-1	-1.89E+0	3.43E-3	NS	2.25E+0
	Beam horizontal	All weather	2556	0.550	-4.84E+0	-1.61E+0	8.35E-3	1.07E-2	1.72E+0
		Clear	741	0.660	-6.44E+0	NS	NS	2.47E-2	2.50E+0
		Fine	806	0.480	-3.71E+0	-5.04E+0	NS	1.80E-2	1.99E+0
		Cloudy	1019	0.301	-1.44E+0	-9.53E-1	6.37E-3	NS	7.43E-1
Instantaneous irradiance [W/m²] from Nov. 25,'99 to Oct. 31,'00 at Fukuyama University	Global	All weather	2954	0.708	-7.34E+2	-4.94E+2	3.05E+0	NS	7.47E+2
		Clear	757	0.899	1.77E+2	5.13E+2	-1.29E+0	NS	1.09E+3
		Fine	780	0.734	-6.37E+2	-7.63E+2	2.63E+0	NS	8.84E+2
		Cloudy	1417	0.498	-5.89E+2	-4.99E+2	3.00E+0	NS	5.19E+2
	Beam horizontal	All weather	1835	0.622	-2.38E+3	-1.04E+2	4.72E+0	4.29E+0	4.86E+2
		Clear	708	0.809	-1.11E+3	NS	NS	4.02E+0	7.20E+2
		Fine	665	0.598	-2.66E+3	NS	4.64E+0	5.40E+0	4.91E+2
		Cloudy	462	0.350	-2.14E+3	NS	4.19E+0	4.28E+0	2.44E+2

(NS: the independent variable is not a significant predictor.)

Table 2 Precision of the multiple regression models of irradiance

		Preliminary analysis (All weather)				Weather condition analysis (Clear+Fine+Cloudy)			
		RMSD		MBD		RMSD		MBD	
Cumulative irrad. [MJ/m²h]	Global	0.399	26%	0.000	0.0%	0.374	24%	0.001	0.1%
	Beam Horizontal	0.496	60%	-0.001	-0.1%	0.456	55%	0.007	0.9%
Instantaneous irrad. [W/m²]	Global	145	41%	5	1.4%	137	38%	2	0.5%
	Beam Horizontal	136	54%	42	16.7%	129	51%	42	16.7%

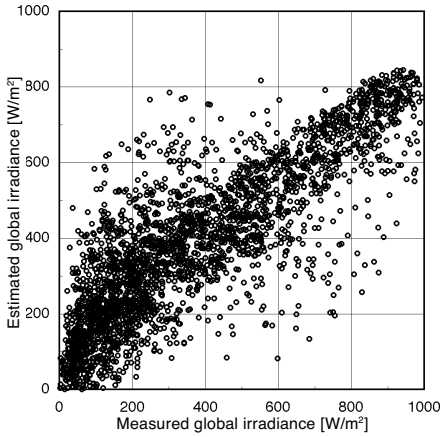

Figure 5 Measured and estimated instantaneous global irradiance by preliminary analysis

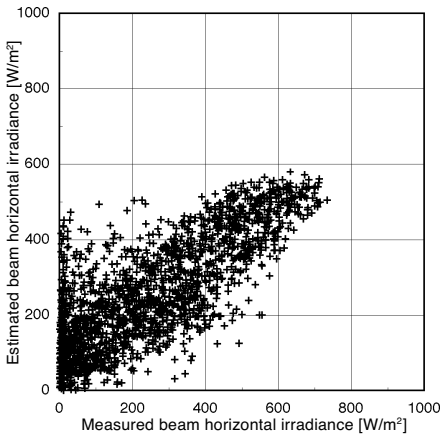

Figure 6 Measured and estimated instantaneous beam horizontal irradiance by preliminary analysis

channel [9], in which the precision was about 30% on the global radiation and 60% on the beam radiation.

The percent RMSD values of the global model indicate that the instantaneous model is less precise than the cumulative model. This suggests that the spatial average of satellite data could correspond to the temporal average of surface data. The low resolution of the satellite images, i.e. 6.7 km/pixel, spatially averages the cloud cover and cloud type in a moment, while the surface observed cumulative data are temporal average at a point on the ground.

Weather condition analysis

The database of 2954 cases is divided into three subsets according to the normalized albedo A_{nVS} as the index of weather condition [10, 11]:

(a) *Clear* ($A_{nVS} \leq 0.15$) 757 cases

(b) *Fine* ($0.15 < A_{nVS} \leq 0.25$) 780 cases

(c) *Cloudy* ($0.25 < A_{nVS}$) 1417 cases

Where the visually observed cloud amount c_o classifies the weather conditions, i.e. *Clear* ($c_o = 0, 1$), *Fine* ($c_o = 2, 3, ...8$) and *Cloudy* ($c_o = 9, 10$).

The multiple linear regression analysis for the global and beam horizontal irradiance are executed on the three subsets of the database respectively using equations (2) and (3). As the results, R square values and partial regression coefficients for the multiple linear regression are shown in Table 1. **Figure 7** and **Figure 8** show the comparison of measured and estimated instantaneous global and beam horizontal irradiance by the

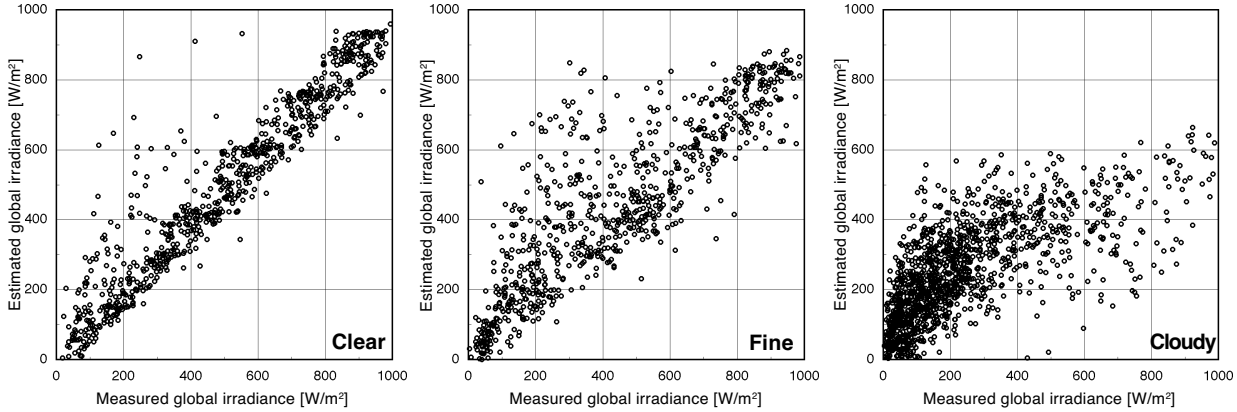

Figure 7 Measured and estimated instantaneous global irradiance by weather condition analysis

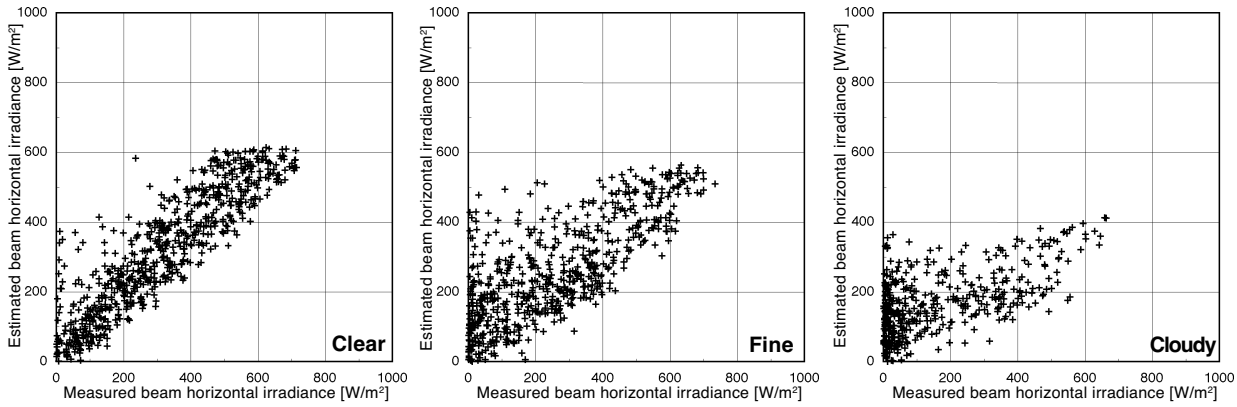

Figure 8 Measured and estimated instantaneous beam horizontal irradiance by weather condition analysis

weather condition analysis. The precision of the models are shown in Table 2.

Table 1 shows that the instantaneous global component depends on the sine of solar elevation angle $\sin h_s$, the normalized albedo A_{nVS} and the equivalent black body temperature T_{bIR}, while the beam horizontal component depends on $\sin h_s$ and both the equivalent black body temperature T_{bIR} and T_{bWV}.

In Table 2, the mean bias difference (MBD) of the instantaneous beam horizontal irradiance is relatively large. From the scatter plots shown in Figure 8, the cause is considered as follows. When the weather condition is *Cloudy* (the cloud amount c_o = 9, 10), the sun sometimes appears through a rift in the clouds, then the measured beam horizontal irradiance I_{oBH} may make a jump beyond 400 [W/m²]. In this case, however, the corresponding pixel of the satellite image is almost covered by the cloud, and estimated beam horizontal irradiance I_{eBH} never reach 400 [W/m²]. This also happens to the global components shown in Figure 7. On the other hand, when a small fragment of cloud covers the sun in the *Clear* sky (c_o = 0, 1), the measured beam horizontal irradiance I_{oBH} may fall down though the estimated beam horizontal irradiance I_{eBH} remains high. In the *Fine* sky condition (c_o = 2, 3,...8), both the over-

Table 3 Coefficients of the multiple regression models of illuminance

			Cases	R^2	k	B_1	B_2	B_3	B_4
Instantaneous illuminance [klx]	Global	All weather	2954	0.713	-7.53E+1	-5.05E+1	4.55E-1	-1.55E-1	8.66E+1
		Clear	757	0.888	-1.08E+1	NS	NS	NS	1.20E+2
		Fine	780	0.745	-1.17E+2	-6.09E+1	4.44E-1	NS	1.03E+2
		Cloudy	1417	0.517	-7.61E+1	-5.74E+1	3.76E-1	NS	6.41E+1
	Beam horizontal	All weather	1821	0.620	-2.83E+2	5.97E-1	4.51E-1	-9.42E+0	6.07E+1
		Clear	709	0.789	-1.42E+2	-5.68E+1	NS	5.34E-1	8.88E+1
		Fine	651	0.609	-3.26E+2	NS	6.03E-1	6.12E-1	6.21E+1
		Cloudy	461	0.340	-1.83E+2	NS	6.87E-1	NS	3.07E+1

(NS: the independent variable is not a significant predictor.)

Table 4 Precision of the multiple regression models of illuminance

		Estimated (All weather)				Estimated (Weather cond.)			
		RMSD		MBD		RMSD		MBD	
Instantaneous illuminance [klx]	Global	16.8	40%	0.5	1.2%	16.0	38%	0.2	0.5%
	Beam Horizontal	16.1	56%	4.7	16.5%	15.1	53%	4.5	15.7%

estimation and underestimation may happen as shown in Figure 7 and Figure 8. This consideration agrees with the very low MBD of the cumulative beam horizontal irradiance in Table 2.

To improve the precision of the instantaneous model, not only the cloud amount but also the cloud type should be derived from the satellite images to improve the accuracy of the weather classification which currently bases on the normalized albedo only. This will be dealt in the further study to classify the cloud amount and cloud type by combining the normalized albedo and the equivalent black body temperature .

Daylight source model

For the daylighting simulation, the instantaneous illuminance data for the specific time and location are usually required to estimate the worst scenario of the luminous environment. In the same way as the irradiance model above mentioned, the multiple linear regression equations are examined to estimate instantaneous global illuminance E_{eG} [klx] and the beam horizontal illuminance E_{eBH} [klx].

$$E_{eG} = k_G + b_{1,G} A_{nVS} + b_{2,G} T_{bIR} + b_{3,G} T_{bWV} + b_{4,G} \sin h_s \quad (4)$$

$$E_{eBH} = k_B + b_{1,B} A_{nVS} + b_{2,B} T_{bIR} + b_{3,B} T_{bWV} + b_{4,B} \sin h_s \quad (5)$$

Table 3 shows the coefficients of the multiple regression models. **Table 4** shows the precision which gives an outline similar to the instantaneous irradiance.

APPLICATION: ESTIMATION OF GEOGRAPHICAL DISTRIBUTION OF DAYLIGHT AVAILABILITY

The daylight source model mentioned above is applied to estimate the geographical distribution of global and beam horizontal illuminance along the broken line of 90 pixels shown in **Figure 9**. Figure 9 also plots the places of the Fukuoka Meteorological Observatory (130˚23'E, 33˚35'N) and the Fukuyama University (133˚15'E, 34˚30'N). **Figure 10** shows the profile of IR, WV and VS image values along the broken line. It is assumed that the coefficients of the daylight source model in Table 3 are applicable to the areas along the line, because most areas are located in the same climatic zone, the Seto Inland Sea Climate, where the climate is relatively mild and the sea is calm. **Figure 11** illustrates the result of global and beam horizontal illuminance. Such simulation technique will be useful to estimate the total gain of solar energy in a region when solar systems come into wide use in the near future.

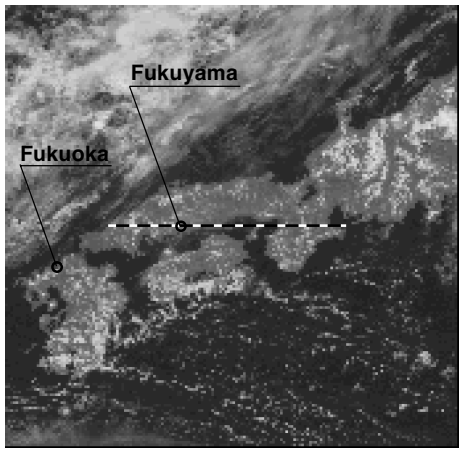

Figure 9 Fukuoka and Fukuyama in Western Japan plotted on the visible image taken from Figure 1

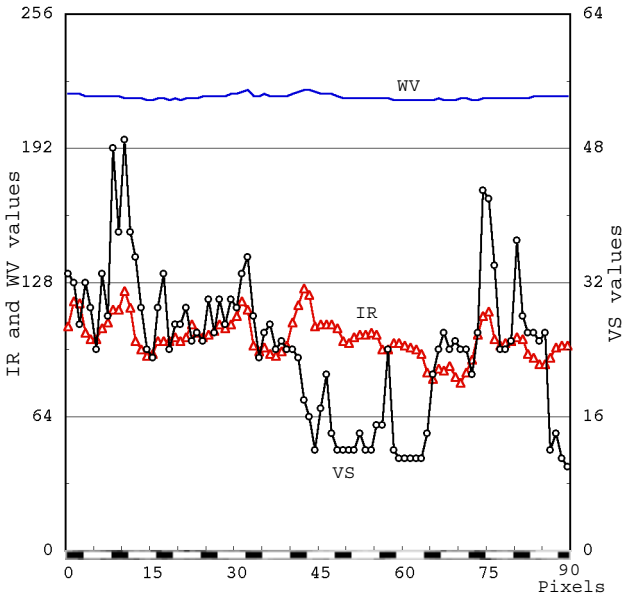

Figure 10 Profile of the IR, WV and VS image values along the broken line shown in Figure 9

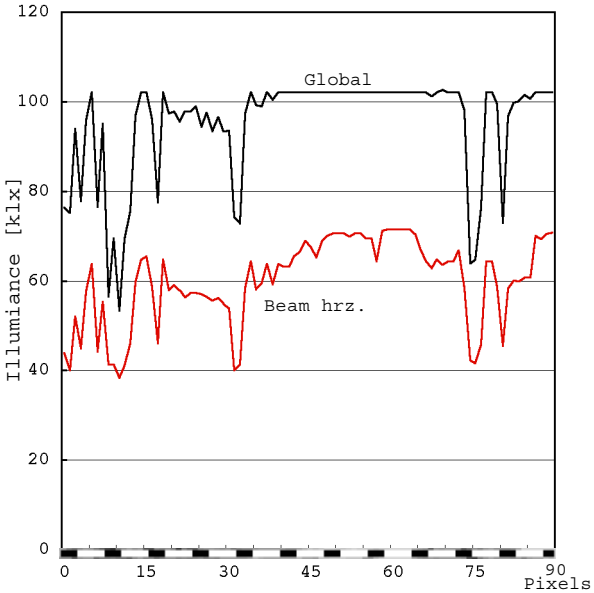

Figure 11 Global and beam horizontal illumninance estimated from image values shown in Figure 10

CONCLUSIONS

The author proposed a statistical model for global and beam solar radiation using the three channels of geostational meteorological satellite images. The model is based on the multiple linear regression analysis to estimate surface observed hourly cumulative global and beam radiation values from the satellite observed image values.

The purpose of this paper is to examine the precision of the model. The multiple liner regression analysis is performed between the satellites image values and instantaneous irradiance measured at the Fukuyama University. By the preliminary analysis for all weather condition, or regardless of weather condition, the precision expressed by the percent RMSD values for instantaneous irradiance are 41% for the global and 54% for the beam component. The overall precision agrees with an elaborate model based on visual channel in which the precision was about 30% on the global radiation and 60% on the beam radiation. The weather condition analysis improves in the percent RMSD values. The percent MBD values of the beam irradiance are relatively low. The causes reducing the precision are studied to improve it in the further study.

The multiple liner regression analysis is also performed between the satellites image values and instantaneous global and beam illuminance. As an application, the daylight source model estimates geographical distribution of global illuminance and beam horizontal illuminance.

ACKNOWLEDGMENTS

This work was supported by the Grant-in-Aid of the Ministry of Education, Science and Culture (12450236 & 12650605), and the TOSTEM Foundation for Construction Materials Industry Promotion. The image processing was performed using the public domain NIH Image program written by Wayne Rasband at the U.S. N.I.H.

REFERENCES

1. Akasaka Y. et al.: Expanded AMeDAS Weather Data, Maru-zen, 2000 (in Japanese).
2. Tarpley J. D., ''Estimating incident solar radiation at the surface from geostationary satellite data'', J. Applied Meteorology, Vol.18, pp.1172-1181, 1979.
3. Gautier C., Diak G. and Masse S., ''A simple physical model to estimate incident solar radiation at the surface from GOES satellite data'', J. Applied Meteorology, Vol.19, pp.1005-1012, 1980.
4. Cano D., Monget J. M. , Albuisson M., Guillard H., Regas N. and Wald L., ''A Method for the Determination of the Global Soar Radiation from Meteorological Satellite Data'', Solar Energy, Vol.37, No.1, pp.31-39, 1986.
5. Diabate L., Demarcq H., Regas N. and Wald L, ''Estimating incident solar radiation at the surface from images of the earth transmitted by geostationary satellites: the Heliosat project'', Int. J. Solar Energy, Vol.5, pp.261-278, 1988.
6. Perez R., Seals R., Stewart R., Zelenka A., Astrada-Cajikal V., ''Using satellite-derived insolation data for the site/time specific simulation of solar energy systems'', Solar Energy, Vol.53, No.6, pp.491-495, 1994.
7. Fontoynont M., Dumortier D. et al., ''Satellight: a European programm dedicated to serving daylight data computed from Meteosart images'', Lux-Europa Conference, Amsterdam, pp.1-12.1997.
8. Beyer, H. G., Costanzo C., Heinemann D., "Modifications of the Heliosat Procedure for Irradiance Estimates from Satellite Images", Solar Energy, Vol.56, No.3, pp.207-212, 1996.
9. Ineichen P., Perez R., "Derivation of Cloud Index from Geostationary Satellites and Application to the production of Solar Irradiance and Daylight lluminance Data", Theor. and Appl. Clim., Vol.64, pp.119-130, 1999.
10. Uetani Y., ''Prediction of the Global and Beam Irradiance and Illuminance by the Geostational Meteorological Satellite Images'', Special Volume, 24th Session of the CIE, Warsaw, p p.51-54,1999.
11. Uetani Y.: "Simulation of Daylight Performance of Buildings by the Daylight Source Model based on Geostational Meteorological Satellite Images", Proceedings of Building Simulation'99 in Kyoto, pp.547-553, 1999.
12. JMBSC, ''The Meteorological Satellite Monthly Report'', July 1996 - June 1997.
13. Kidder S. Q. and Vonder Haar T. H., ''Satellite Meteorology-an Introduction'', Academic Press, 1995.

NOMENCLATURE

h_s Solar elevation angle [˚].

I_{oG} Global irradiance [W/m^2] observed by the pyranometer

I_{oBN} Beam normal irradiance [W/m^2] observed by the pyrheliometer with solar tracker

I_{oBH} Beam horizontal irradiance [W/m^2] derived as $I_{oBH} = I_{oBN} \sin h_s$

E_{oG} Global illuminance [klx] observed by the global illuminance meter

E_{oBN} Beam normal illuminance [klx] observed by the beam illuminance meter with solar tracker

E_{oBH} Beam horizontal illuminance [klx] derived as $E_{oBH} = E_{oBN} \sin h_s$

A_{VS} Albedo derived from VS image, [-]

A_{nVS} Normalized albedo derived from A_{VS} and $h_{s,}$ [-]

T_{bIR} Equivalent black body temperature derived from IR image, [K]

T_{bWV} Equivalent black body temperature derived from WV image, [K]

I_{eG} Estimated global irradiance [W/m^2]

I_{eBH} Estimated beam horizontal irradiance [W/m^2]

E_{eG} Estimated global illuminance [klx]

E_{eBH} Estimated beam horizontal illuminance [klx]

$k_G, b_{1,G}, b_{2,G}, b_{3,G}, b_{4,G}$ Constant and partial regression coefficients in the multiple linear regression equation for I_{eG} or E_{eG}.

$k_B, b_{1,B}, b_{2,B}, b_{3,B}, b_{4,B}$ Constant and partial regression coefficients in the multiple linear regression equation for I_{eBH} or E_{eBH}.